We are IntechOpen, the world's leading publisher of Open Access books Built by scientists, for scientists

6,900
Open access books available

185,000
International authors and editors

200M
Downloads

Our authors are among the

154
Countries delivered to

TOP 1%
most cited scientists

12.2%
Contributors from top 500 universities



WEB OF SCIENCE™

Selection of our books indexed in the Book Citation Index in Web of Science™ Core Collection (BKCI)

Interested in publishing with us?
Contact book.department@intechopen.com

Numbers displayed above are based on latest data collected.
For more information visit www.intechopen.com



Chapter 5

Phonon Dispersions as Indicators of Dynamic Symmetry Reduction in Superconductors

Jose A. Alarco and Ian D.R. Mackinnon

Additional information is available at the end of the chapter

http://dx.doi.org/10.5772/intechopen.79216

Abstract

Strong correlations between phonon energies and superconducting transition temperatures can be extracted from phonon dispersion calculations using density functional theory for a range of superconducting materials. These correlations are robust and consistent with experimental data for key external conditions including isotope effects, elemental substitutions and pressure variations. Changes in the electronic band structure also correlate with transitions to/from superconductivity but, in general, are less sensitive and less obvious than phonon behaviour. A computational approach that considers both phonons and electrons and the presence or absence of a phonon anomaly works well for conventional superconducting materials with hexagonal, cubic or tetragonal symmetries. Superconductivity in these compounds often involves symmetry reduction in an original non-superconducting parent compound induced, for instance, by substitution or by a dynamic reduction in symmetry shown in electron density distributions and Raman spectra. Such symmetry reduction is effectively modelled with super-lattice constructs which link Raman spectra with key superconducting parameters.

Keywords: density functional theory, metal diboride, electronic band structure, phonon dispersion, phonon anomaly, Raman spectroscopy, superlattice, superconductivity, transition temperature, deformation potential, Fermi level

1. Introduction

When distant neutral atoms are brought together, they eventually come close enough to form solids. As the atoms approach, the initial gas-like behaviour of the neutral atoms, changes to a correlated atomic liquid-like behaviour first, and then, to more organised collective movements in the periodic, or aperiodic, solid. In a periodic solid, the electrons involved in the

IntechOpen

© 2018 The Author(s). Licensee IntechOpen. This chapter is distributed under the terms of the Creative Commons Attribution License (http://creativecommons.org/licenses/by/3.0), which permits unrestricted use, distribution, and reproduction in any medium, provided the original work is properly cited. CC BY

ionic cores of the atoms retain much of their localised structure pertaining to their original neutral atoms, but the outer valence electron orbitals begin to overlap, forming bonds that stabilise the structure, if the right conditions are met [1]. Valence electrons also provide conduction electrons that can move around in the case of metals, and essentially, regulate overall collective behaviour [2]. In a metal, the valence electrons now become the entities with gas-like behaviour, following the Fermi-Dirac statistics for particles with spin ½ [3], instead of Maxwell-Boltzmann statistics [4].

The gas of valence electrons is not static and neutral; and is, in fact, more like a plasma, capable of collective motion to shield out variations in electrostatic potential caused by the motion of ions [5]. This behaviour is evident when the Born-Oppenheimer approximation is valid; a fundamental concept in density functional theory (DFT) [6, 7]. In this approximation, the positions or distributions of these outer electrons adjust very quickly in response to any ionic core movements [3, 8]. Furthermore, on the basis of Fermi-Dirac statistics and the exclusion principle, most of the electrons under the influence of external fields remain in the same states. Only a small fraction in the thermal layer (with energy k_BT from the Fermi energy E_F, where k_B is equal to the Boltzmann constant) are free to move [5], provided these electrons can find empty states to move to and that energy and momentum conservation laws are fulfilled.

1.1. Valence electrons

The movement of nearly free valence electrons in a metallic solid is generally well described by Bloch waves, which invoke periodicities in the crystal lattice. Again, this assertion is particularly true for systems subject to the Born-Oppenheimer approximation. The collection of energies of allowed quantized Bloch states is grouped together in the *electronic band structure*, which correspond to the solutions of Schrodinger's equation typically displayed in reciprocal space as a function of the wave vector k [3, 9]. Similarly, the equations for atomic or ionic core movements can be solved for the vibrational (or phonon) states and the allowed frequencies are grouped together in the *phonon dispersion*. In order to differentiate vibrational states from electronic states, the former and the latter are typically labelled with q and k, respectively. However, both q and k have the same formal periodic properties [9].

In the case of silicon or diamond, which have a two-atom basis in the lattice, or for more complex compounds with different atomic species, acoustic and optic branches evolve [3, 10]. The difference between acoustic and optic branches in phonon dispersions, particularly in monoatomic cases such as silicon or diamond, is quite similar to the difference between bonding and antibonding states in the electronic spectrum [9]. The frequencies in the phonon dispersion are related to the interatomic bonding forces or energies, and when the calculated phonon dispersions contain negative frequencies (or not), this can be considered an indicator of dynamic or structural stability or instability [7, 11, 12]. This indicator is particularly useful for analyses of situations that are difficult to replicate in the laboratory, such as for solids at very high pressures [7].

The Born-Oppenheimer approximation allows for the separation of variables in the equations of movement for electrons and for ionic cores [3, 8], and gives distinct electronic band structures and phonon dispersions. However, the two concepts are not completely independent, particularly for superconducting solids, such that the *electron–phonon interaction* often should be considered [3]. An electron–phonon coupling is dependent on the density of states in

proximity to the Fermi energy and is relatively strong for electronic bands with a high density of states adjacent to the Fermi energy [13]. Such coupling is important for explanations of a wide range of physical properties, including superconductivity [3] and especially that of the conventional Bardeen-Cooper-Schrieffer (BCS) type [14].

1.2. Lattice dynamics

Atoms in a crystal lattice participate in two types of oscillations of different nature [2]: (i) thermal oscillations, for which amplitudes and energy change with temperature become zero at T = 0 K; and (ii) zero oscillations, which exist even at T = 0 K and are of quantum mechanical origin related to Heisenberg's uncertainties. If the amplitude of zero oscillations are commensurate with the mean distance between atoms, then a crystalline structure cannot be formed at normal pressure, even at T = 0 K, and the substance will remain liquid [2]. Another important subset of the thermal oscillatory motion is given by the Debye temperature, Θ_D, which is determined by the ratio between the thermal and the bonding energies. At low temperatures (below Θ_D), the bonding energy promotes the coordinated motion of atoms and only the low frequency lattice waves are excited, while at higher temperatures (above Θ_D) the movement is more chaotic and all lattice waves are excited. In both cases, the equilibrium positions remain approximately in the same places [2, 15]. The concept of a high Θ_D has played a significant role in the historical understanding of superconductivity [16].

Raman spectroscopy of crystalline solids is one of the techniques that can provide direct estimates of the electron–phonon interactions, where an incident, monochromatic laser beam excites electrons, and as a result of interactions that are, in general with phonons, an inelastically scattered beam with a shifted frequency or wavenumber is detected. The Raman activity of phonon modes can be determined with reference to group symmetry analyses for the periodic crystal [10, 17]. Although, in fact, the structure of a crystalline compound is not strictly periodic in each given instant of time because of the oscillating motion of ions [2].

DFT offers the capability to calculate electronic bands and phonon dispersions with great accuracy and, more recently, within viable computation time given rapid progress with software codes and computer hardware. As a result, DFT is now an essential tool to assist with interpretation of experimental results. With continued success and more rigorous agreement between experimental and calculated results, DFT is now established as a reliable tool for accurate prediction of material properties. Furthermore, DFT is an effective computational technique for *ab initio* prediction of a new material's stability and of the potential to engender key properties such as superconductivity.

Of perhaps greater importance is the potential to predict the superconducting transition temperature, T_c, in anticipation of experimental measurement. We will demonstrate that this capacity is inherent in the fundamental attributes of DFT and that the practice is readily applied. We will use examples of existing materials to demonstrate the approach and provide reference to predicted "new superconducting materials" that are yet to be synthesised. Determination of a value for T_c is not only important to minimise the disappointment of synthesising an infertile haystack to find the elusive needle but also to plan for practical evaluations of superconducting applications. However, perhaps of even greater significance is the exceptional value of insight into the mechanisms and underlying interactions from which superconductivity emerges [18, 19].

For simple structures, the Eliashberg theory—modified via the McMillan or Allen-Dynes equations—determines T_c from electron–phonon couplings using normal state parameters [20] reasonably well. Given this, it should be possible for standard DFT models to provide all the necessary superconducting characteristics of a material from a knowledge of the crystal structure. In this chapter, we explore how Raman spectroscopy can reveal the dynamic symmetry of superconducting materials, and how consideration of lower symmetry superlattice modes provides clues to materials behaviour. We will show how the energy of key phonon modes shows strong correlation with the value of T_c for MgB_2, the archetype superconducting metal diboride, as well as for compositional analogues in the symmetry group.

2. MgB_2: unique characteristics

Magnesium diboride, MgB_2, is an electron–phonon coupled BCS-type superconductor with the highest superconducting transition temperature T_c for this structure type at ~40 K [21]. The material is a simple compound with only three atoms (two boron and one magnesium) in an hexagonal unit cell with P6/mmm symmetry and lattice parameters a = 3.086A and c = 3.524A [21, 22]. This simple structure with atoms in the second row of the Periodic Table and extensive microstructural and physical property characterisation, makes MgB_2 ideal for DFT calculations that can be experimentally validated [23, 24].

A wide variety of microstructural, chemical and physical properties of MgB_2 have been thoroughly investigated and the reader is referred to example review papers on the topic [24]. Investigations on MgB_2 include studies using high quality crystals and polycrystalline materials, on isotopic effects ([25, 26], and references there in), on hydrostatic pressure effects ([11, 27, 28], and references there in), on a variety of metal substituted forms ([29–33], and references there in), and other similar structures that do not superconduct or that have T_c values different to MgB_2. This significant body of work presents experimental data that can be compared with outcomes from DFT calculations [11, 19, 25, 29, 30, 34, 35] and provides validation of structure–property interpretations. **Figure 1** displays a schematic of the MgB_2 structure emphasising the layered nature of the compound.

2.1. Electronic properties

Figure 2a displays the electronic band structure (EBS) of MgB_2 along representative reciprocal space directions for the P6/mmm group symmetry, for the reduced Brillouin zone scheme [9, 36]. The EBS of MgB_2 contains two characteristic approximate parabolas centred at **Γ**, with a common vertex at about 0.4 eV above the Fermi energy, inverted and with different curvatures each of which represents different effective masses (see **Figure 2a**). These parabolas correspond to the σ heavy and light hole bands along the **Γ–K** and **Γ–M** reciprocal directions and are associated with electronic conduction or metallic behaviour in the plane of the boron atoms [37, 38]. Two parallel degenerate lines with low dispersion along the **Γ–A** direction, also associated with the σ bands, is another characteristic feature of the MgB_2 EBS. These σ bands are known to couple strongly with the important E_{2g} vibration modes that correspond to in-plane B–B atom movements and are key to superconductivity in MgB_2. Other bands, not identified as σ bands, are primarily π bands and relate to three-dimensional movement of electrons [37, 38].

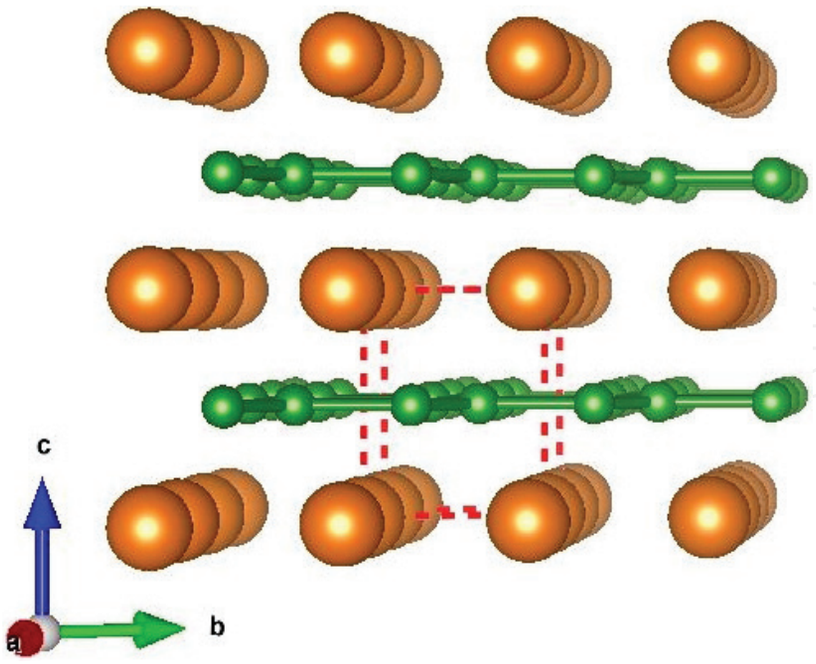


Figure 1. Schematic of the MgB_2 crystal structure in perspective view showing the layered nature of the compound. Metal atoms are gold colour and boron atoms are green; red dotted lines outline a unit cell.

The σ band parabolas at **Γ**, after folding from the extended Brillouin zones back into the reduced zone scheme are identified schematically in **Figure 2a** as red and blue lines. This folding of one suite of bands around **Γ** is exemplified in **Figure 2a** as extended orange dotted lines and, for more generic bands, is recognised in a number of key publications [39, 40]. The nature of these bands, and the observation that after folding the bands are nearly full, is a strong indication that the Fermi energy is large (compared with other AlB_2-type structures) and that valence electrons associated with these bands completely fill the first Brillouin zone.

The coexistence in MgB_2 of inverted, approximate parabolic σ bands and low dispersive bands in the **Γ–M** and **Γ–A** directions, respectively, results in approximately coaxial, parallel σ warped tubes for the Fermi surface when represented in the reduced zone scheme and as shown in **Figure 2b**. These parallel tubes correspond to hole carriers, that is, outside and inside are filled and empty, respectively, with electrons. This creates an inter-tubular volume in the reduced zone scheme, which is filled with respect to the inner tube and empty with respect to the outer tube [35]. This concept is awkward for physical interpretation in reciprocal, let alone real, space and can be more easily reconciled by assuming an extended zone scheme with separate inner or outer diameter tubes at alternating and adjacent reciprocal space points [11, 35]. Thus, the nature of the Fermi surface in MgB_2 with parallel sections in close proximity intrinsically implies resonant behaviour of electrons and phonons.

Calculating the difference in kinetic Fermi energies for the adjacent σ bands, using the respective Fermi vectors and effective masses, results in a value of phonon energy equivalent to approximately twice the energy gap of MgB_2 [38]. Such an energy gap corresponds to a frequency approximating 1/5, or 20%, of the frequency of the E_{2g} mode [25, 34]. This value of vibration frequency is a Raman active mode (after folding the Brillouin zone boundaries to the **Γ** point) for a reduced P6/mmm symmetry for MgB_2 (e.g. the space group $P6_3mc$). A reduced

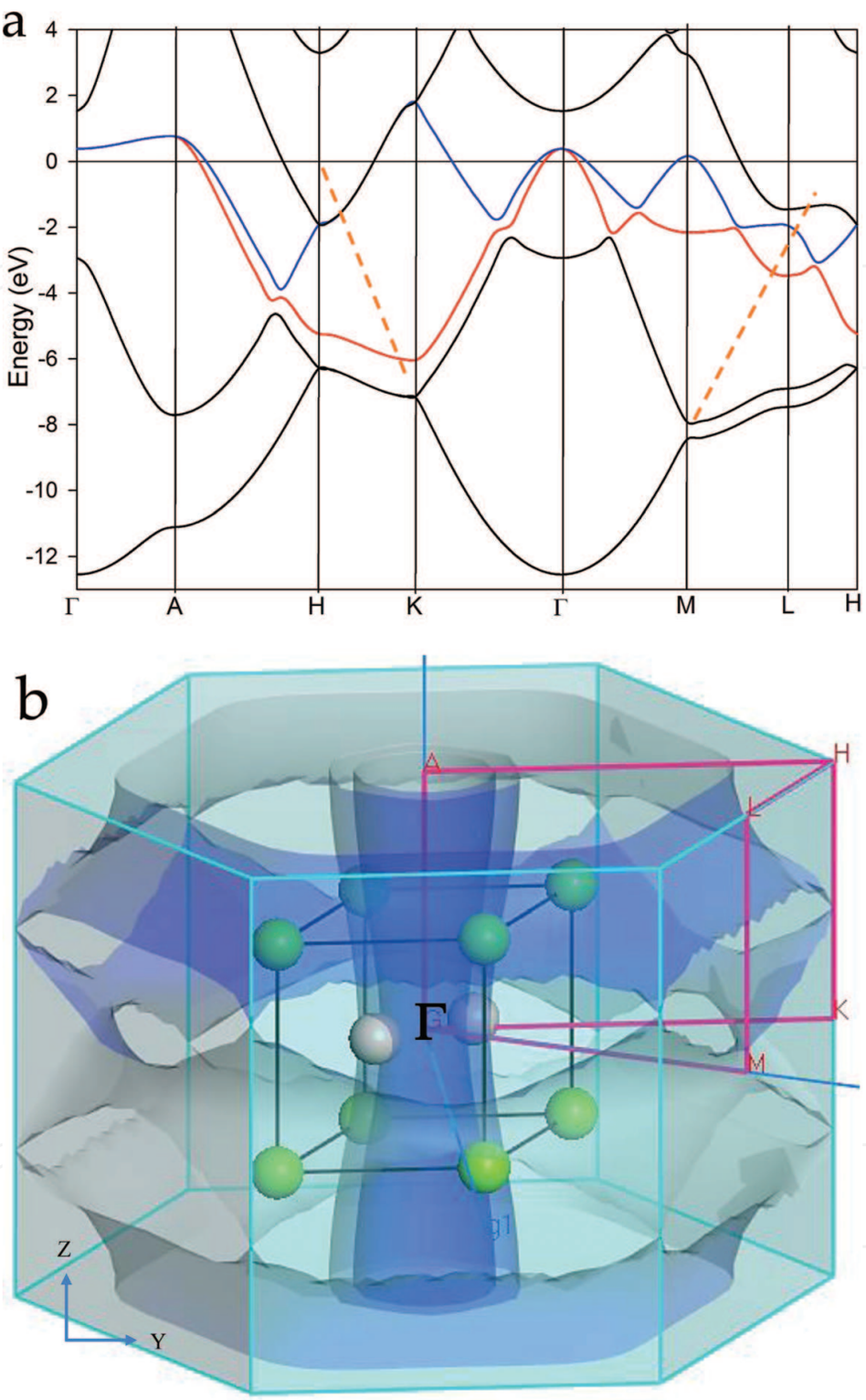


Figure 2. DFT calculated features of MgB_2 using the LDA functional and $\Delta k = 0.02A^{-1}$ showing (a) EBS highlighting the two characteristic parabolas (red and blue lines) centred around **Γ**. The folded nature of the parabolic σ bands identified by the orange dotted lines is discussed in the text; (b) a section of the Fermi surface showing tubular σ surfaces (light and dark blue) vertical segments coaxial with the *c*-axis.

http://dx.doi.org/10.5772/intechopen.79216

symmetry configuration is readily represented by a superlattice along the *c*-axis direction [34]. Such low frequency vibrations have been observed in experimental Raman spectra of MgB_2 ([34], and references there in) which also varies commensurate with the isotope effect [25].

2.2. Vibrational properties

Figure 3 displays the calculated phonon dispersion (PD) for MgB_2 at atmospheric pressure (0 GPa hydrostatic stress). The PD branches for optical phonons are labelled at the **Γ** point. The important E_{2g} modes intersect the **Γ** point at about 550 cm^{-1} wavenumber. The "W shaped" region around the E_{2g} mode at **Γ** below the highest adjacent frequency B_{1g} is called a *phonon dispersion anomaly*. This feature was originally described by Kohn [41] after whom it is named and, for MgB_2, verified experimentally using inelastic X-ray scattering (IXS) [42, 43]. Hence, this "W shaped" feature is not an artefact of the DFT calculations.

As we will indicate later, there are important relationships between features in the EBS and PD of MgB_2 that are perhaps critical to the "tuning" of a structure to induce or enhance superconductivity. We show that the Kohn anomaly is an indicator of superconductivity in—to date—BCS materials [11, 19, 25, 29, 30, 34, 35]. Other features may also be important indicators of resonant behaviour. For example, we note above that the two characteristic parabolas centred at **Γ** show a common vertex at ~0.4 eV above the Fermi energy (**Figure 2a**). In the PD, the Kohn anomaly is also centred at **Γ** with degenerate E_{2g} modes. Of further interest, two other parabolas centred on **A** and **M** above the Fermi level in the EBS also show degenerate E_{2g} modes at the same reciprocal lattice boundaries in the PD. These characteristics imply, *a priori*, that symmetry plays a role in the real space moderation, or distribution, of electrons and phonons in superconducting materials.

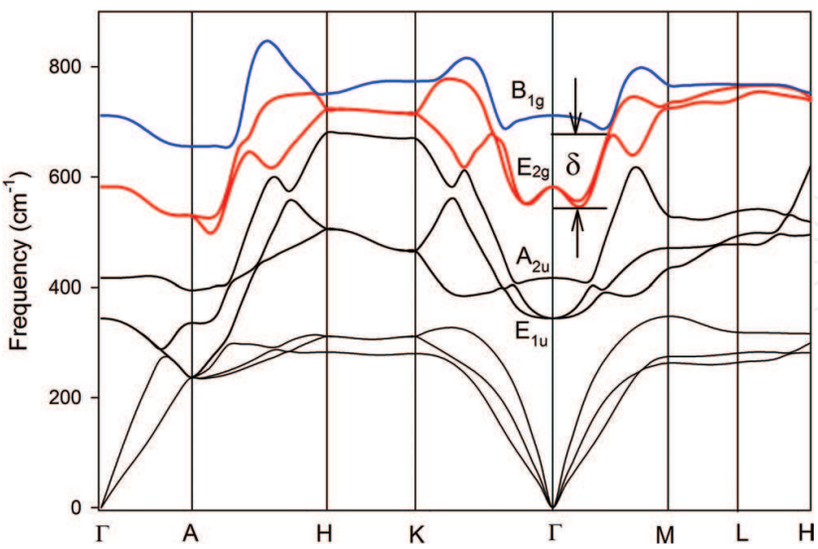


Figure 3. DFT calculated phonon dispersion for MgB_2 at atmospheric pressure. The parameter δ is an important indicator of the phonon anomaly thermal energy.

A temperature, T_δ can be extracted from measurement of the depth of the anomaly (i.e. a value in cm^{-1} for δ in **Figure 3**) [29, 30, 34]. The value for T_δ is strongly correlated with the superconducting transition temperature T_c. The correlation is robust and consistent with experiments under a wide range of external conditions including isotopic [25, 34] and metal substituted compositions of MgB_2 [29, 30], a wide range of hydrostatic pressures [11] as well as for isostructural compounds in the silicate system [30]. In addition, for MgB_2 we have shown that the depth of the anomaly is strongly correlated to the inter-tubular Fermi surface volume [11, 35] and to electron density variations along B–B bonds in response to movement of B atoms linked to the dominant E_{2g} vibration modes [35].

To model phonon dispersions, a practical computational consideration is that the virtual crystal approximation (VCA) is not implemented for plane waves in Materials Studio CASTEP [44]. Therefore, an alternative to representation of atom substitutions in a reduced unit cell structure is to use larger unit cells with substituent atoms in respective proportions. This approach results in a need to construct superlattices to describe metal substitution in MgB_2, albeit the principle may apply to many layered structures.

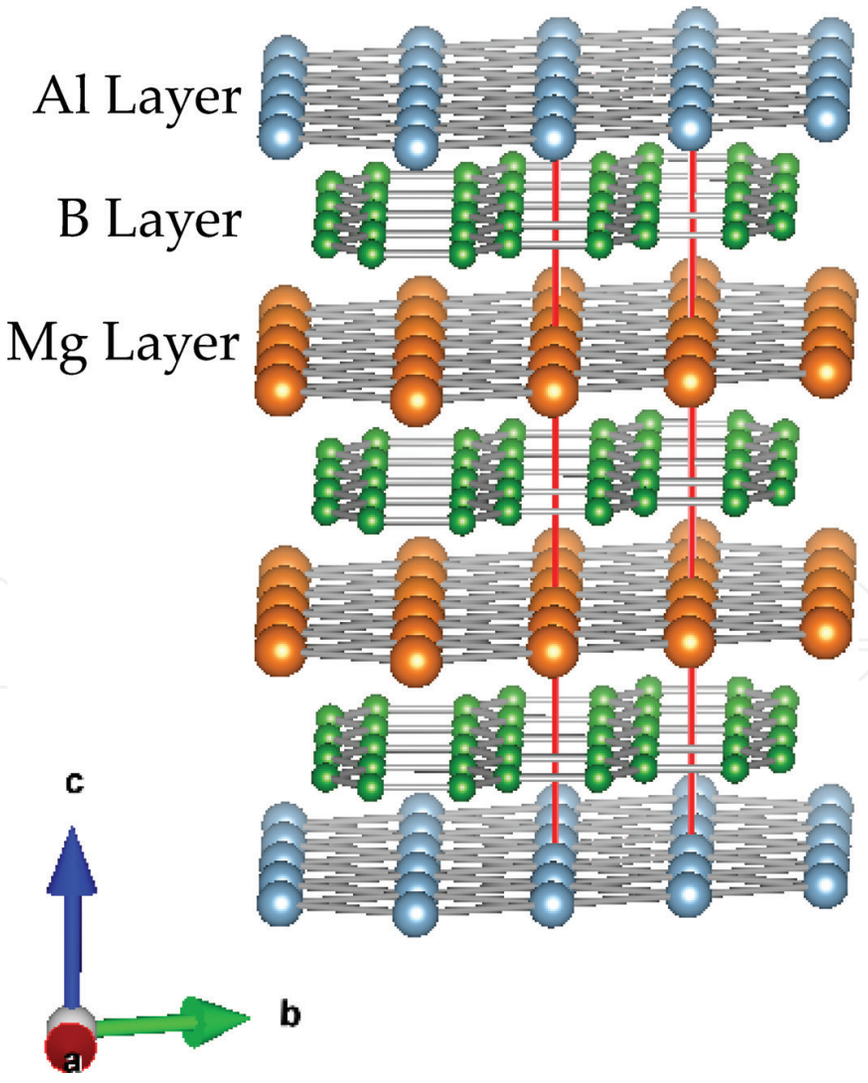


Figure 4. Superlattice construct for Mg_2AlB_6 (Mg:Al::2:1) representing $Mg_{0.67}Al_{0.33}B_2$.

For Al-substituted MgB_2, superlattices in the *c*-axis direction are well described using a range of diffraction and microscopy techniques [29, 45–47] (and references therein). Thus, we use superlattice constructs to describe intermediate compositions of metal-substituted MgB_2 to configure models for band structure and phonon dispersion DFT calculations. **Figure 4** shows a schematic of a superlattice for 0.33 atoms of Al substitution per Mg atom in MgB_2. This principle of a superlattice construct is also used for all other types of metals substituted into the MgB_2 structure in the examples to follow. This approach, when combined with a converged PD calculation, presents an *a priori* validation of potential for phase stability of the specific composition. However, this validation does not infer solubility of the substituted metal in the MgB_2 structure [30].

3. Transition metal diborides

As noted in Section 2, the electronic band structure and phonon dispersion of MgB_2 display unique characteristics that are not necessarily present in other metal diborides except for some metal substituted variations of MgB_2. We will now compare fundamental characteristics of MgB_2 with other diborides containing metal atoms with different valence states and orbital characteristics. **Figure 5** shows the region of the Periodic Table we systematically investigate using DFT calculations of both electronic band structures and phonon dispersions. In this

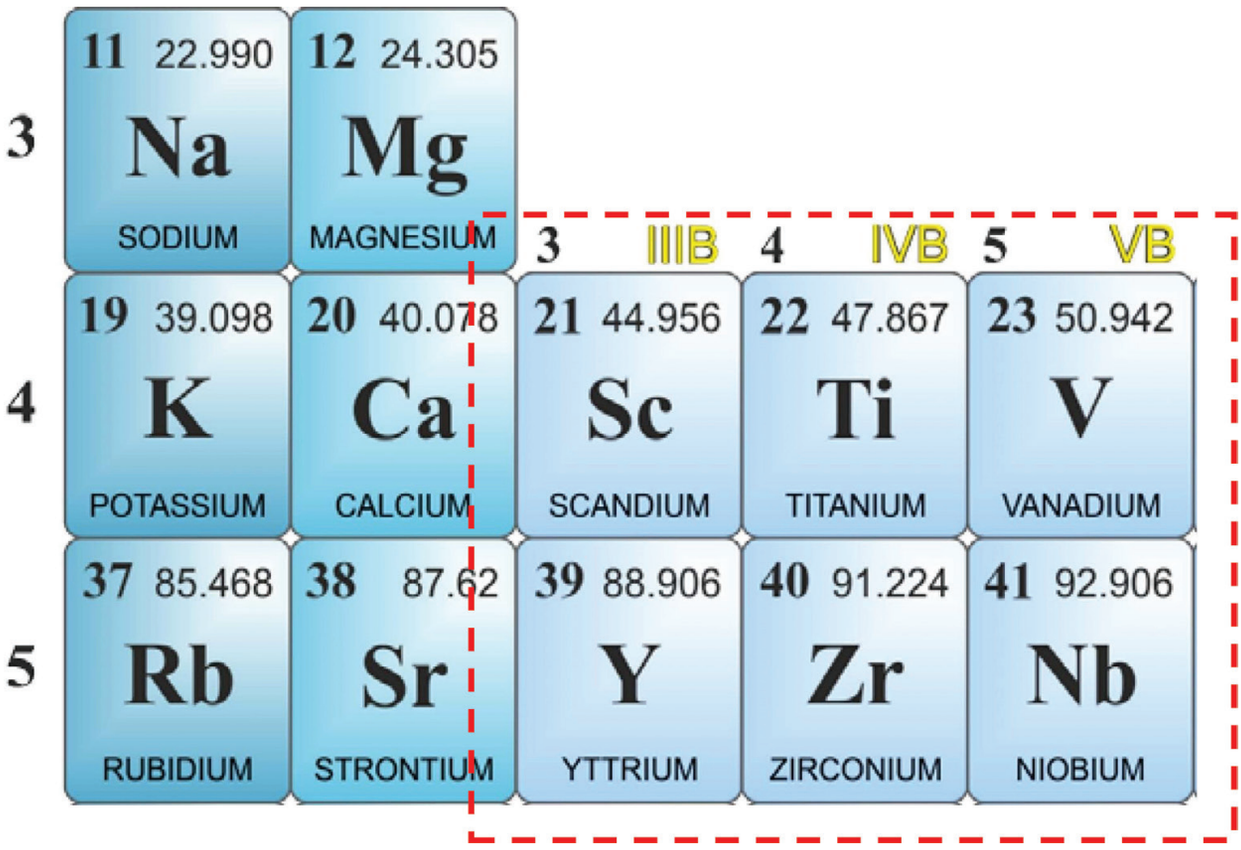


Figure 5. Region of the periodic table with low atomic number transition metals (dotted red outline) investigated using DFT calculations of electronic bands and phonon dispersions.

analysis, we evaluate similarities and differences to MgB_2, in order to identify parameters that control the unique features of superconductivity in MgB_2.

3.1. Row 4 diborides

Figures 6 and **7** display the DFT calculated EBS and PD for the transition metal elements (Z = 21–23; Z = 39–41) identified in **Figure 5**. Of the transition metal diborides shown in **Figures 6** and **7**, ScB_2 shows the most prospective resemblance to MgB_2 albeit with substantially reduced features. Both PDs display depressions or anomalies in their E_{2g} branches near **Γ** from which temperatures can be extracted and correlated with a corresponding T_c [29, 30, 34]. The anomalies derive from co-existing heavy and light effective masses for approximate inverted parabolas in key sections of their EBS. These inverted parabolas are centred above the Fermi level at **Γ** for MgB_2. However, for ScB_2 the inverted parabolas at **Γ** are below the Fermi level yet degenerate bands of an inverted parabola format are also centred at **A**. In addition, the order of optical modes in the PD is different in ScB_2 compared to MgB_2 with the E_{2g} modes at the highest frequency.

This apparent discrepancy in behaviour compared with MgB_2 can be reconciled by considering the signs of the relevant orbitals and their likely contribution to hybrid bonding between boron and the metal atoms along the *c*-direction. Metals in a higher row, including Sc, Ti and V, provide valence electrons from d orbitals while in MgB_2, p orbitals are predominant. While the lobes of p orbitals have opposite signs, those of d orbitals have the same sign. Thus, while hybridization of pure p orbitals in MgB_2 produces a periodic pattern of orbitals in a single unit cell, hybridization of mixed p and d orbitals in ScB_2 requires a double supercell to establish an appropriate periodic orbital pattern.

3.2. Row 5 diborides

As shown in **Figure 7**, the EBS for YB_2 is similar to that shown in **Figure 6** for ScB_2; in particular, the configuration of heavy and light effective masses above the Fermi level at the boundary point **A**. Note also, that as with ScB_2, bands at **Γ** in the EBS are below the Fermi level. A similar evaluation of the respective d orbital contribution to hybrid bonds as noted for ScB_2 may also apply to YB_2. However, the PD in **Figure 7b** does not clearly show an anomaly, but rather displays overlap between two E_{2g} branches; one of which is concave and the other convex in the **Γ–M** and **Γ–K** directions. The reason for this difference in PD between YB_2 and ScB_2 is unclear but may be due to insufficient Δk grid resolution [13]. In addition, the calculation for YB_2 determines a Fermi energy of −1.62 eV, which is often referred to an average zero-point in the interstitial space and may indicate large vacuum regions in the unit cell [48]. Nevertheless, these DFT calculations for YB_2 suggest potential for constructive moderation of conduction properties by conventional materials methods including metal substitution or application of pressure.

Other metal diborides, such as VB_2, TiB_2, ZrB_2 and NbB_2, do not display co-existing light and heavy effective mass σ bands that intersect the Fermi level in their EBS. Therefore, approximately parallel Fermi surfaces and important deformation potentials, which are strongly linked to the superconductivity in MgB_2 and in other compounds, cannot be defined in these

http://dx.doi.org/10.5772/intechopen.79216

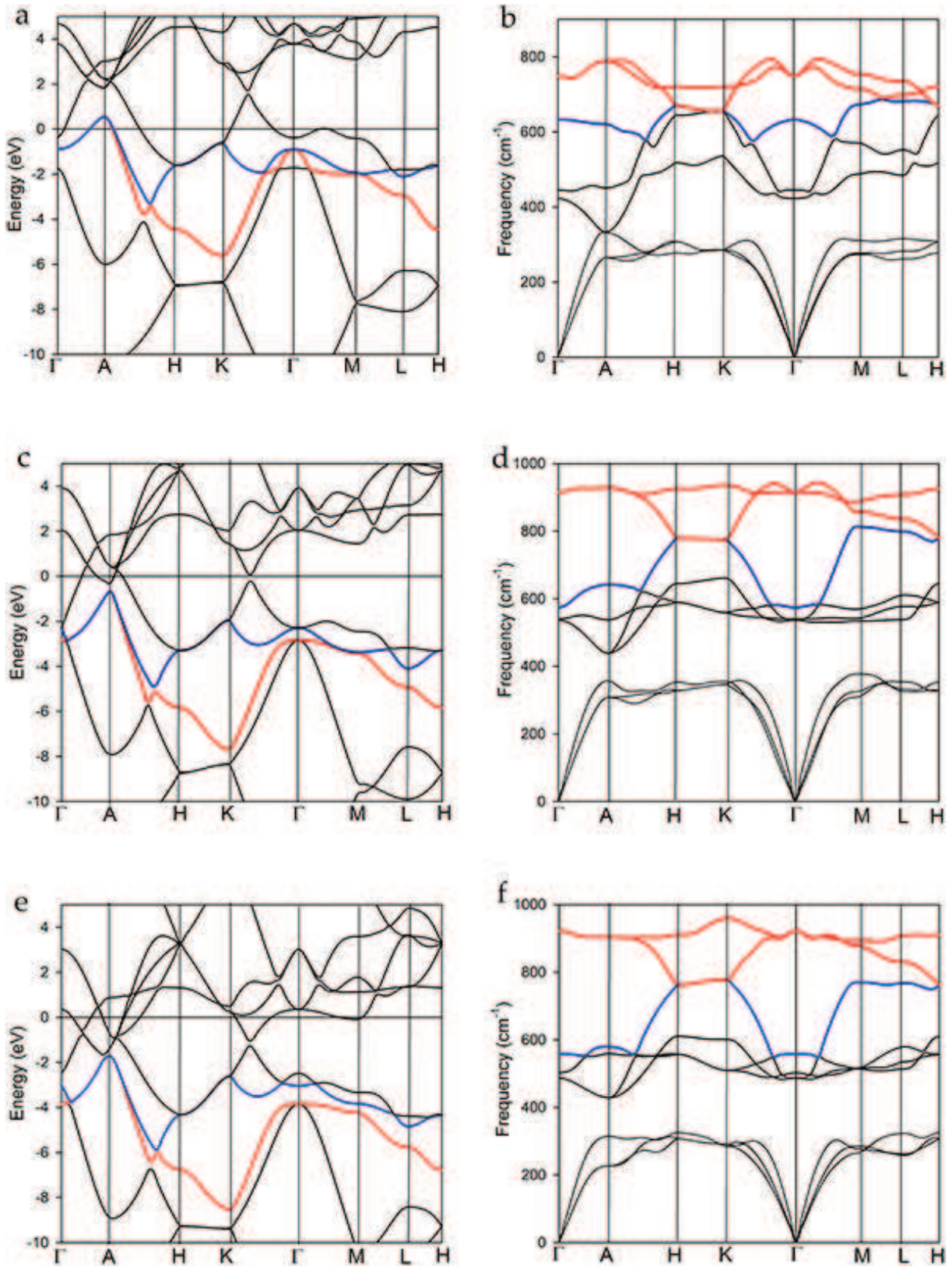


Figure 6. DFT calculated electronic bands and phonon dispersions for the first 3d transition metal diborides. **(a)**, **(c)** and **(e)** shows EBS for ScB_2, TiB_2 and VB_2, respectively, in which the two parabolic bands similar to the σ bands of MgB_2 are identified as red and blue lines; **(b)**, **(d)** and **(f)** shows PDs for ScB_2, TiB_2 and VB_2 respectively, in which E_{2g} (red) and B_{2g} (blue) phonon modes are identified.

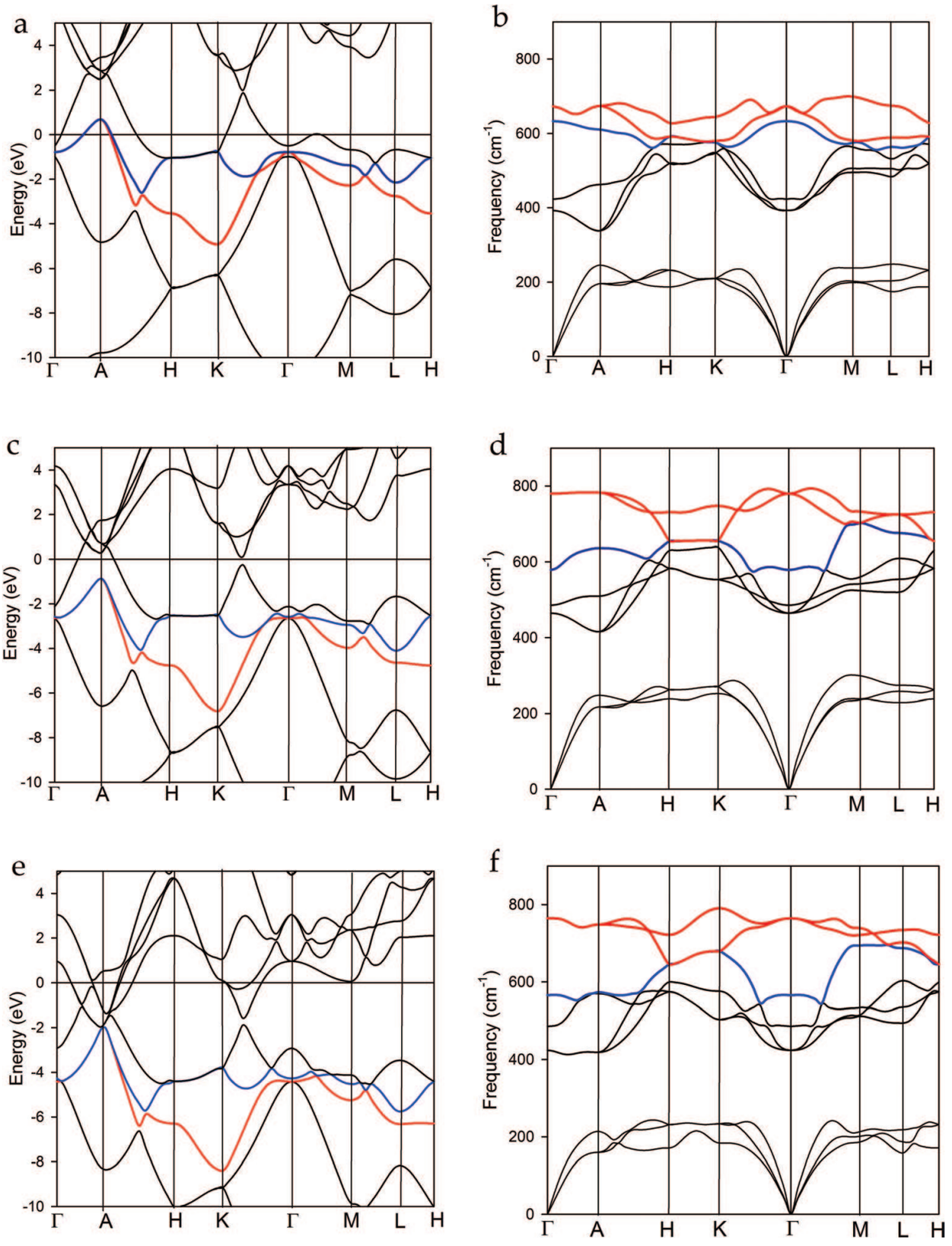


Figure 7. DFT calculated electronic bands and phonon dispersions for the first 4d transition metal diborides. **(a)**, **(c)** and **(e)** shows EBS for YB_2, ZrB_2 and NbB_2, respectively, in which the two parabolic bands similar to the σ bands of MgB_2 are identified as red and blue lines; **(b)**, **(d)** and **(f)** shows PDs for YB_2, ZrB_2 and NbB_2 respectively, in which E_{2g} (red) and B_{2g} (blue) phonon modes are identified.

cases. Therefore, these compounds are unlikely to be superconducting without some modification (e.g. element doping or substitution) and do not display anomalies in their phonon dispersions. Such modification to the structure type, for example, adding boron to form $NbB_{2.5}$ [49], or substituting other elements, such as in $Zr_{1-x}V_xB_2$ [50–52] or $Zr_{1-x}Nb_xB_2$ [53] leads to superconductivity; as also suggested by Pickett et al. [54] based on DFT calculations of AlB_2-type structures. These minor modifications to the stoichiometry of an MB_2 structure are excellent examples of "fine-tuning" that achieves a dramatic change in material property. We surmise that this fine-tuning would be manifest in the EBS as coexisting σ bands shifting to above the Fermi level and the appearance of a Kohn anomaly in a PD centred around **Γ**.

3.3. Diboride fine tuning

Strategic utilisation of DFT models allows snapshots of dynamic electron interactions in solids. An and Pickett [55] used DFT to determine deformation potential—or the energy required to break the degeneracy of σ electronic bands per unit length of inter-bond distances—in superconductors. This work also showed that for MgB_2, the E_{2g} phonon modes are of greater significance for superconductivity than other optical phonon modes in this structure; confirming many other experimental studies at the time. To utilise this approach, the electron density (ED) distributions of relevant bonds are determined at discrete steps of atom displacements along a bond direction. The computational technique requires calculation of the EBS for a particular frozen atom configuration with due consideration of symmetry conditions invoked by the displaced atom positions [35]. For MgB_2, the structure affords an uncommon opportunity to evaluate deformation potentials along the direction(s) of the E_{2g} mode which parallel the B–B bonds in the *a*-*b* plane.

As boron atoms are displaced from their equilibrium positions, a degeneracy at the vertex of the inverted σ band parabolas is broken and a deformation potential is created [55]. A critical displacement is identified where the lower effective mass σ band becomes tangential to the Fermi level. At this point, the σ band becomes filled and can no longer take part in electron transitions between the heavy and light σ bands. Thus, coherency is lost and superconductivity is destroyed [35]. An example of this condition is shown in **Figure 8a** in which the EBS for atom displacement, $D_x = 0.006$ (or a change of ~3.5% of the bond length after converting from fractional values of the *a*-lattice parameter) along the E_{2g} mode is shown compared with the equilibrium positions (blue lines) for boron atoms in MgB_2 [35]. **Figure 8b** shows the region around **Γ** in greater detail depicting the relative shift of each band and the loss of degeneracy with atom displacement.

The PDs for models of deformation potential for diboride structures show corresponding shifts in the phonon anomaly with displacement of atoms along the E_{2g} mode directions [35]. **Figure 8c** and **d** shows a partial PD for the **Γ–K** and **Γ–M** orientations of MgB_2 at equilibrium and at $D_x = 0.006$ relative displacement of boron atoms from equilibrium. At the critical displacement (**Figure 8d**), the E_{2g} mode is similar in energy to the B_{2g} mode, as if the total (temperature or kinetic) energy associated with the anomaly has been stored into deformation potential energy. In addition, the E_{2g} modes are clearly non-degenerate in these orientations, including **Γ**, for atom displacement $D_x = 0.006$ (**Figure 8d**). The difference in Fermi energies between the critical displaced position and the equilibrium position also shows a strong correlation with the superconducting energy gap [35].

The bond charges, which are highly localised along the covalent bond positions, display modulations which can be interpreted as superlattices of dynamic charge distribution [35]. Because the charge that is transferred between bonds is a fraction of the total bond charge, the superlattice modulation is subtle and may not be resolved by conventional diffraction techniques that typically reflect average models of atomic structures. Higher intensity and/or resolution probes, such as synchrotron radiation and time resolved experiments, may be required to detect these subtle modulations of charge distribution.

ScB_2 shows features in the PD that suggest superconductivity occurs at low temperature (**Figure 6b**) and experiment shows that the T_c for ScB_2 is 1.5 K (as reported by Sichkar and Antonov [56]). However, as shown in **Figure 6a**, the inverted parabolas around **Γ** in the EBS are degenerate but ~1 eV below the Fermi level. A comparison of the full ScB_2 EBS with MgB_2 (blue lines) and a more detailed view of the region around **Γ** is shown in **Figure 9a** and **b**, respectively. The potential to invoke band tuning, whereby substitution of another element

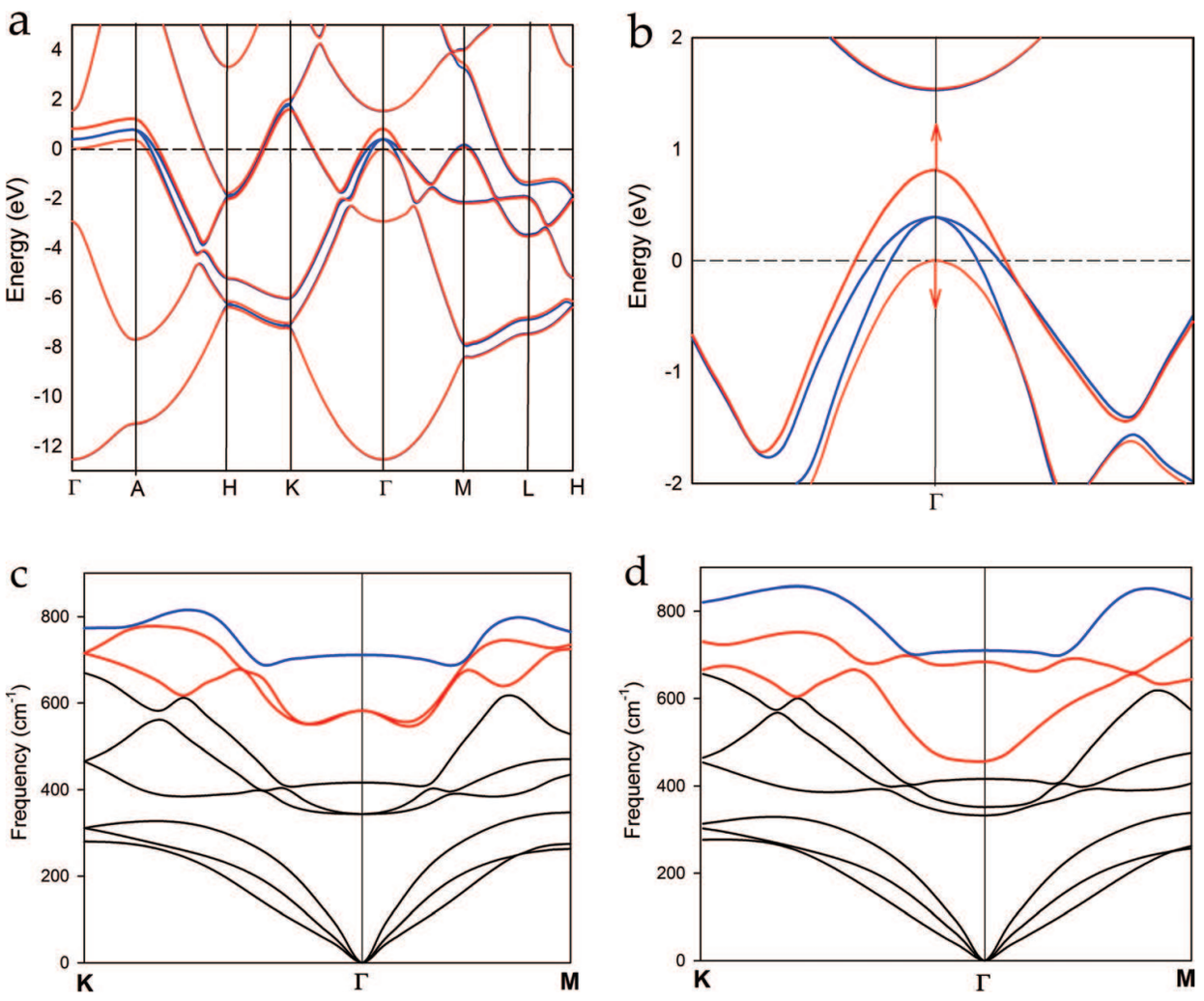


Figure 8. EBS using the LDA functional with $\Delta k = 0.02$ A^{-1} for (a) for MgB_2 at equilibrium (blue) and with relative atom displacement $D_x = 0.006$ (red) along the E_{2g} mode direction (i.e. the B–B bond); (b) enlarged view around **Γ** showing the shift of σ bands causing loss of degeneracy. Partial PD for MgB_2 calculated using the LDA functional for $k = 0.01$ A^{-1} in the **Γ–K** and **Γ–M** orientations showing changes in the E_{2g} (red) and B_{2g} (blue) modes under conditions of (c) equilibrium for $D_x = 0.0$ and (d) with atom displacement $D_x = 0.006$.

http://dx.doi.org/10.5772/intechopen.79216

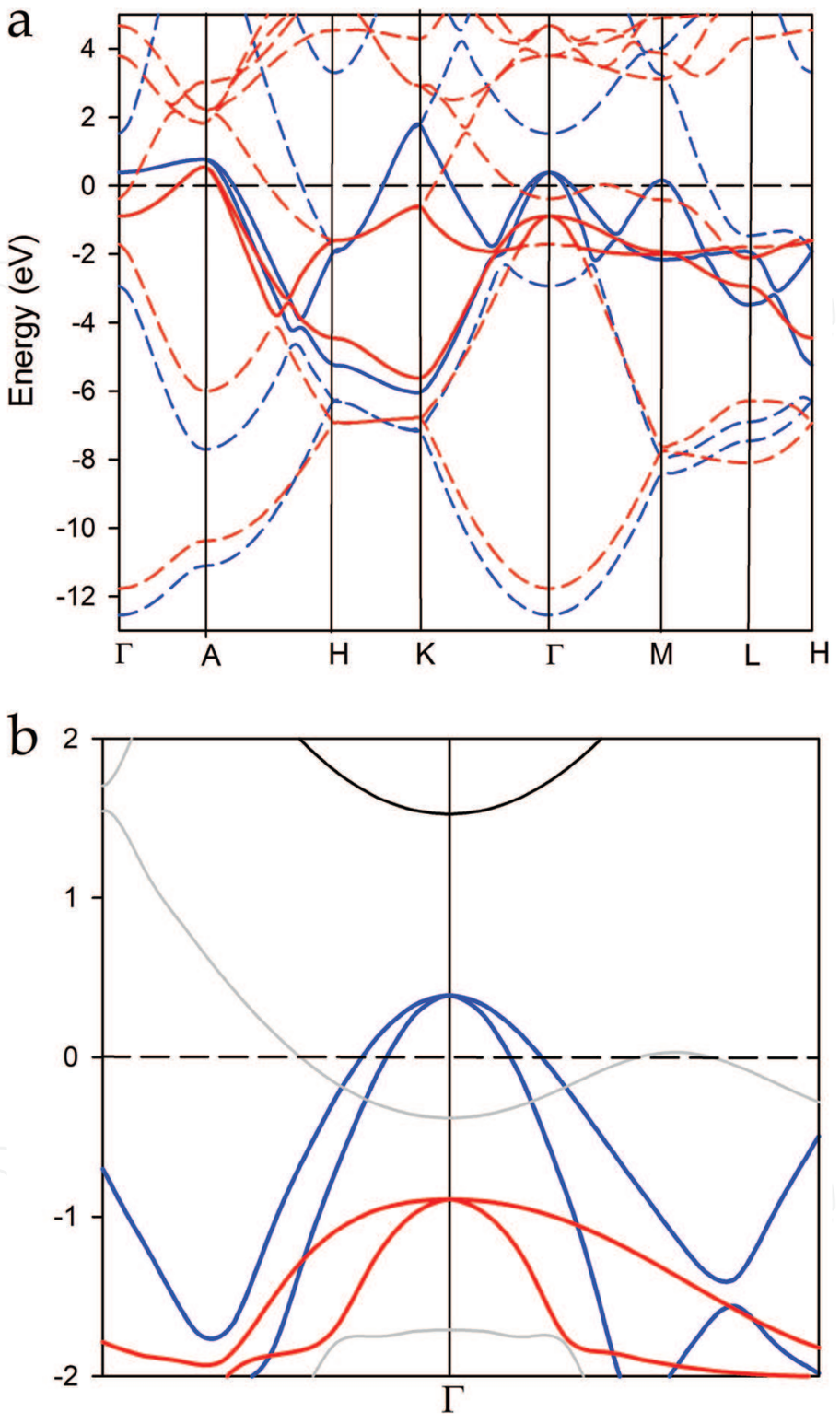


Figure 9. (a) EBS using the LDA functional with $\Delta k = 0.02$ A^{-1} for MgB_2 (blue) compared with ScB_2 (red) showing degenerate parabolas at **Γ** above and below the Fermi level, respectively; note the degenerate parabola for ScB_2 centred around **A**; (b) enlarged view for MgB_2 (blue) and ScB_2 (red) around **Γ**.

for Sc shifts the degenerate parabolas above the Fermi level, may be a viable strategy to achieve a higher T_c for $Sc_{1-x}M_xB_2$. Experiment shows that Sc substitutes for Mg in $Mg_{1-x}Sc_xB_2$ [32] and, in general, is superconducting for $x < 0.3$ [33]. Calculations on the variation of phonon anomaly

with substitution of Sc in MgB_2 show a similar correlation between T_δ and experimentally determined T_c [30].

Figure 8 and similar comparisons in other work [30, 55] show that, in general, PDs are more sensitive indicators of change in electron–phonon coupling, or electron distribution [35], than EBS. This sensitivity to change—either via complete or partial substitution of the metal ion into the structure—is also evident in the comparative energy shifts in phonon modes and the order of modes with change of composition. For example, the type structure for this suite of materials is AlB_2 for which the E_{2g} mode is at the highest frequency (~950 cm^{-1} at **Γ**) and the B_{2g} mode is significantly lower in energy (~500 cm^{-1} at **Γ**) [30]. In addition, the PD for AlB_2 does not show an anomalous form for any optical mode while the EBS shows σ band parabolas at **Γ** and degenerate bands along **Γ–A** below the Fermi level. In comparison, substitution of Mg into the type structure clearly shifts both the phonon modes—reversing the order and frequencies of E_{2g} and B_{2g} (~580 and ~710 cm^{-1} at **Γ**)—and the σ bands albeit the change with the latter is less obvious to the casual observer. For ScB_2, a similar behaviour is evident: an anomaly with degenerate E_{2g} modes at **Γ** and along **Γ–A** in the PD and symmetric, degenerate σ band parabolas around **A** and **Γ** (above and below the Fermi level, respectively; **Figure 6a** and **b**). Again, the change in behaviour for ScB_2 from the type structure, AlB_2, is more evident via the PD.

4. MgB_2: low-frequency Raman peaks

Experimental syntheses of MgB_2 by vapour [57] or solid state [31, 58] methods are well documented in the literature and, in comparison to syntheses of many other superconductors, are uncomplicated. Commercial production of MgB_2 wires [59, 60] was achieved soon after the publication by Nagamatsu et al. [21]. Nevertheless, there are cautionary notes about synthesis of high quality MgB_2 [31, 61, 62]; a particularly relevant matter for Raman spectroscopy because different microstructures can be formed due to small changes in processing conditions (see Figure 2 in Ref. [34]).

In a comparative study of morphologies produced under similar conditions [34], large, micron-sized aggregates containing interpenetrating, euhedral grains of MgB_2 displayed more peaks than those reported in prior Raman characterizations of MgB_2 [34]. Importantly, the signal/noise ratio for these aggregates under identical conditions was significantly higher than the plate morphology aggregates which recorded a lower T_c value of 38.0 K [63]. The quality of Raman signal from the aggregates of euhedral MgB_2 grains with T_c = 38.5 K [63], enabled detection of Raman peaks at low frequencies. Unlike Raman spectra of MgB_2 single crystals targeting specific polarizations oriented along particular crystallographic axes [64, 65], a non-specific geometry with quality, randomly oriented grains presents a modified, atypical response compared to conventional Raman spectra.

By inspection, the most obvious interpretation of atypical Raman spectra is the activation of extra peaks, including those at lower frequencies [34]. These extra peaks suggest that the well-known P6/mmm symmetry determined by bulk techniques may be incorrect or perhaps may indicate a lower symmetry condition. As is known, highly symmetric structures are expected

to have a high number of degeneracies compared with a monoclinic or triclinic structure. As the symmetry of a particular structure is lowered, some degeneracies can be broken and, for example, additional peaks may appear in Raman spectra. In addition, the bulk powder XRD patterns for these MgB_2 samples are consistent with the accepted P6/mmm symmetry. Thus, if symmetry reduction is a viable interpretation of Raman spectra, the effect would likely be subtle and related to a sub-group of the P6/mmm space group. Of note, careful and sophisticated XRD techniques have been used to show that superlattices do occur in MgB_2 [66].

DFT interpretation of the Raman spectra shows that all the observed frequencies, except the low frequency values (i.e. less than ~300 cm^{-1}) are, in fact, part of the list of possible frequencies for MgB_2 [34] with P6/mmm symmetry or related symmetry sub-groups. Raman activity changes between modes depending on the particular sub-group of P6/mmm. Further reduction of the symmetry required a double supercell in the *c*-axis direction to represent all elements of symmetry. When calculations include a superlattice structure for MgB_2, all relevant frequencies are reproduced and additional frequencies, including the low frequencies, match experimental values measured using Raman and IR [34].

In essence, modes that are part of the zone boundary at **A** in the reciprocal lattice representation of the PD (i.e. parallel to the *c*-axis direction) are folded at the mid-point to that boundary for the lower symmetries, and therefore, become part of the **Γ**-point modes of a 2*c*-superlattice. This interpretation of symmetry breaking for MgB_2 is instructive, not only because of the consistent explanation provided to experimentally determined Raman and IR spectra, but also because it allows for additional refinements in understanding. For example, the mode frequencies for MgB_2 can be grouped, to a first approximation, as multiples of a harmonic frequency that shows a clear relationship to the superconducting energy gap [25, 34]. This basic frequency is equal to the pitch or slope of the linear proportionality of harmonic modes and is demonstrated for the obvious case of boron isotopes in MgB_2 [25].

5. Extrinsic influences on MgB_2

There are many external factors that influence superconductivity in MgB_2; the most obvious of which is temperature. The maximum value of a computational modelling program is, *a priori*, to predict behaviour of a material under specific conditions. The capacity to predict the temperature at which a solid transitions to a superconducting state is not an unreasonable demand on DFT when used carefully. Two other extrinsic influences on superconductivity well founded on experimental data are elemental substitution and pressure. For example, the influence of substituent elements, including metals, on the value of T_c for many superconducting families including the cuprates and chalcogenides is well known [67–69]. In addition, pressure applied to single atom metals was first demonstrated in the 1920s and subsequently, led to discovery of 22 elemental solid superconductors [70]. We now briefly describe how attention to PDs and EBSs using DFT modelling provides excellent correlation with experimentally determined superconducting properties for metal substituted MgB_2 and for MgB_2 under pressure.

5.1. Metal substitution

The solubility of other metal atoms in MgB_2, that is, the substitution of Mg within the structure by some other metal, is limited yet well-studied [31, 71, 72] in the wake of Nagamatsu et al. work [21]. Substitution by Al extends to more than 0.5 formula units (e.g. $(Mg_{0.5}Al_{0.5})B_2$) while significant proportions of Sc [32, 33] and Ti [73] are known to substitute into MgB_2. Other elements such as Li, Mn and Fe will substitute for Mg but at much lower amounts as stable phases (e.g. Li < 0.11 formula units) [31]. In nearly all cases, substitution of a metal for Mg in the structure results in a lower T_c compared with the T_c for MgB_2 [30]. Exceptions may be the Ba, Rb and Cs substitutions reported to increase T_c above 40 K by Palnichenko et al. [74], determined using ac susceptibility.

A DFT evaluation of Al substitution in MgB_2 [29] requires the use of superlattices to build a range of $Mg_{1-x}Al_xB_2$ compositions as described in Section 2. PDs for a series of Al-substituted compositions show that the Kohn anomaly changes as Al content is increased. The value of δ decreases with increased Al content. As shown in **Figure 10**, the EBS for $Mg_{0.5}Al_{0.5}B_2$ shows similar format to the MgB_2 parabolic bands that are degenerate at **Γ** and also along **Γ–A**. However, these bands are shifted to lower energy, and ultimately to below or at the Fermi level, with increased substitution of Al for Mg in the structure. For $Mg_{0.5}Al_{0.5}B_2$, the degenerate bands at **Γ** are parallel with the Fermi level which suggests that superconductivity for this composition is minimal or that the T_c is very low. The PD for $Mg_{0.5}Al_{0.5}B_2$ shows a small but measureable anomaly, δ, that provides a T_δ ~ 4.5 K [29] and reiterates the intrinsic value of evaluating both the EBS and PD of superconducting materials.

Using the same methodology noted earlier, the calculated value for thermal energy of the anomaly also reduces consistently with experimentally determined values of T_c, within estimated errors [29]. A plot of T_δ calculated from the change in depth of the phonon anomaly in Al substituted MgB_2 compared with the experimentally determined T_c for similar compositions is shown in **Figure 11** [29]. This example, and others with the AlB_2-type structure [29, 30] demonstrate that *ab initio* DFT modelling can provide consistent and predictable data on the presence/absence of superconductivity for BCS-type materials. In addition, parameters extracted from these models correlate well with experimental data on T_c without requirement to *post-facto* adjust well-known proximal equations.

A computational limitation of this approach is the number of integer superlattice constructs that can be reasonably accommodated within the constraints of multi-user high performance computing facilities to evaluate a wide range of substituted compositions. Nevertheless, with careful attention to experimental details, the same approach has been applied to estimate the T_δ for Sc and Ti substituted MgB_2 [30]. Again, as with Al-substituted MgB_2, the calculated T_δ obtained from measuring the depth of the phonon anomaly correlates very well—within systematic errors—with the experimental values of T_c determined for each composition [29, 30].

http://dx.doi.org/10.5772/intechopen.79216

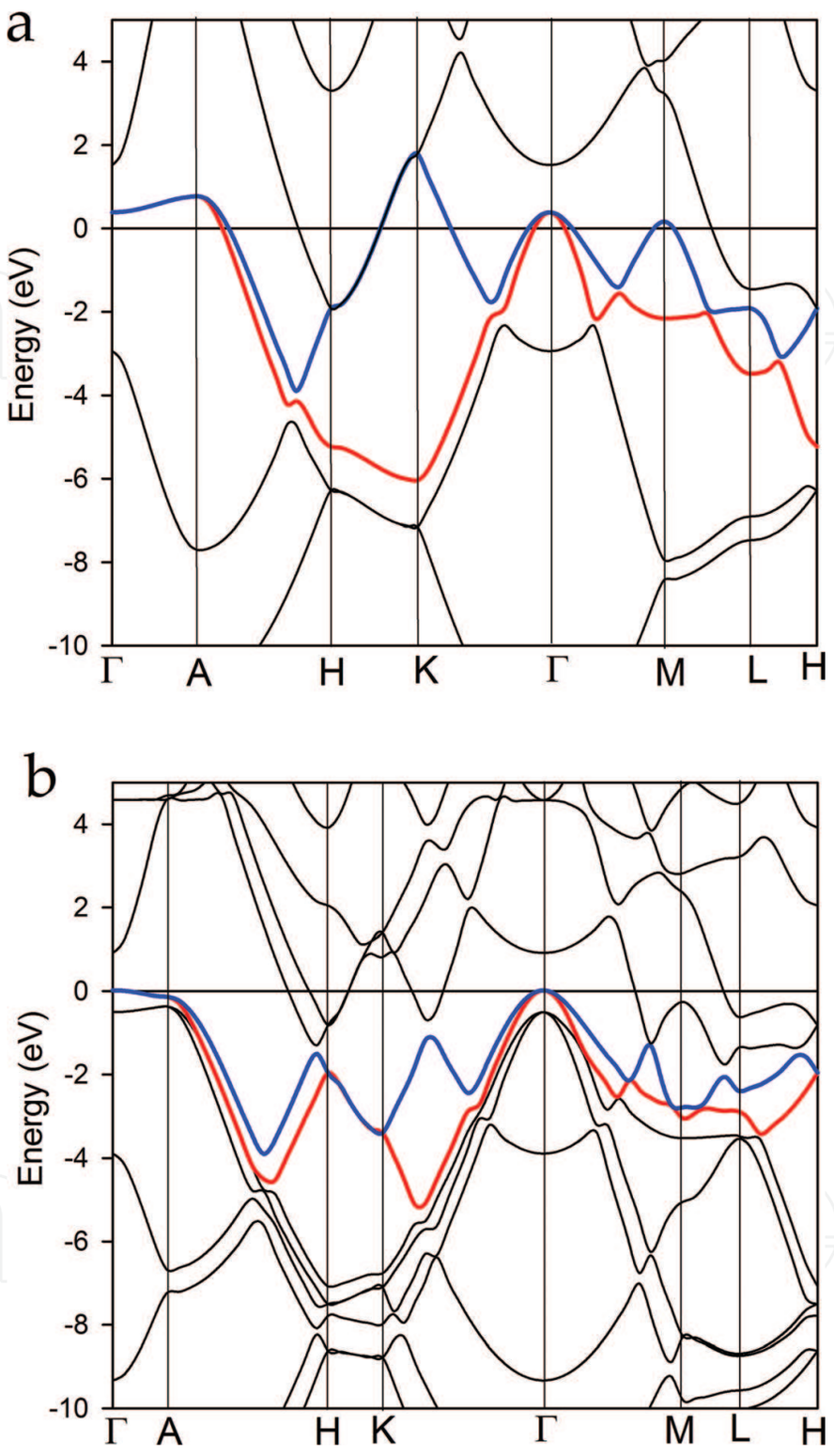


Figure 10. EBS calculated using the LDA functional with $\Delta k = 0.01$ A^{-1} highlighting the two key parabolic bands (blue and red lines) degenerate at **Γ** and along **Γ–A** for (a) MgB_2 and (b) $Mg_{0.5}Al_{0.5}B_2$. In comparison to MgB_2, the superlattice construct for $Mg_{0.5}Al_{0.5}B_2$ results in multiple bands and differences in the relative widths of reciprocal dimensions (e.g. **H–K** and **M–L**) that encompass *c*-axis directions. The degenerate bands at **Γ** for $Mg_{0.5}Al_{0.5}B_2$ are parallel with the Fermi level suggesting a lower value for T_c compared with MgB_2.

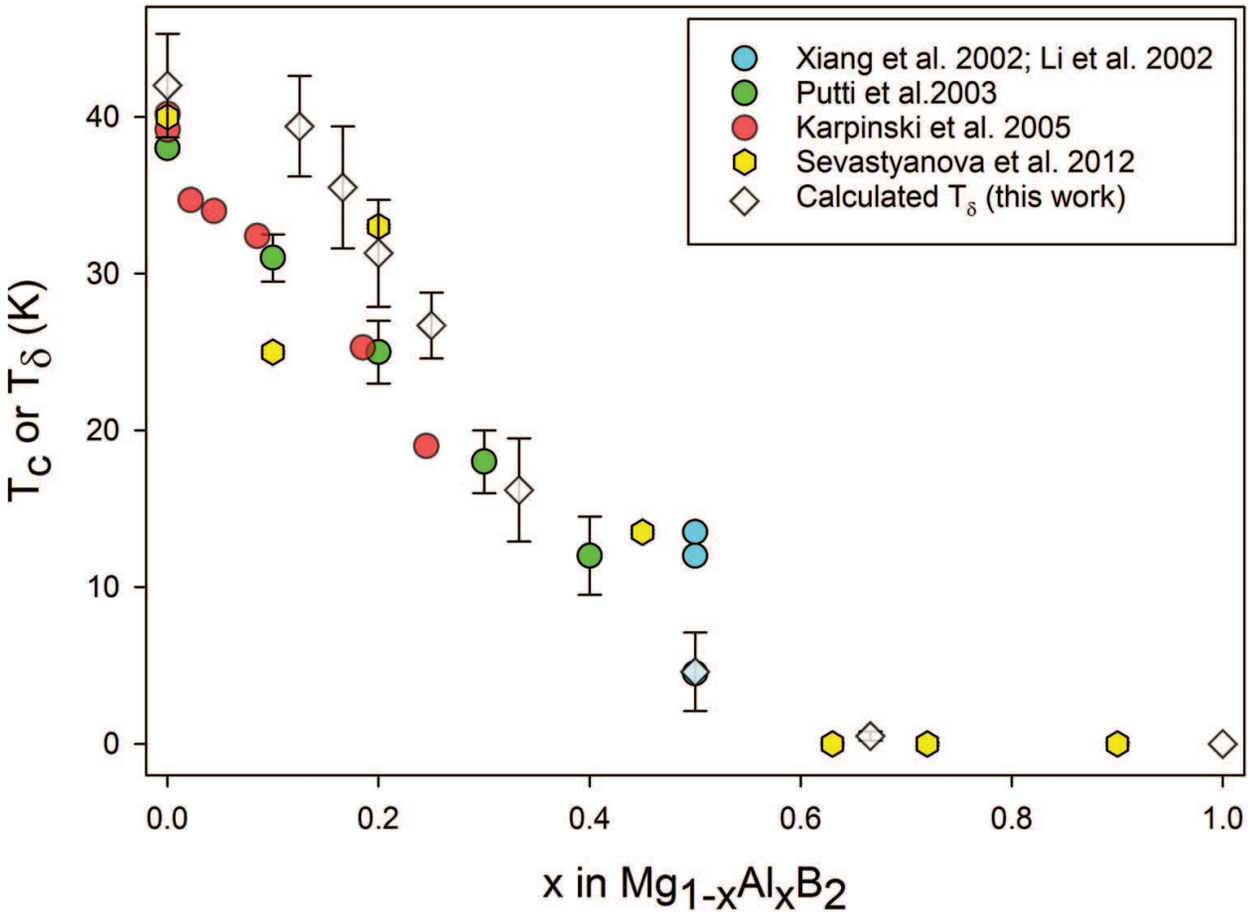


Figure 11. DFT calculated values for T_δ (unfilled diamonds) based on the depth of the phonon anomaly, δ, for Al-substituted MgB_2 compared with experimentally determined values (filled symbols) for T_c (reproduced from [29]).

5.2. Hydrostatic pressure

Application of hydrostatic pressure to many superconducting materials results in a change in the value of T_c [70]. For many materials, increased hydrostatic pressure results in a decreased T_c compared with ambient conditions although care is required with the experimental conditions to apply pressure [27]. For MgB_2, there is abundant experimental work ([11], and references therein) on the pressure dependence of T_c including Raman and lattice parameter variations up to ~57 GPa [75, 76]. Similar pressure effects can be determined using *ab initio* DFT and, more importantly, the effects of pressure changes on EBS and PDs are demonstrable [11], noting that hydrostatic pressure is one of the few external pressure conditions for which PDs can be calculated [44].

Figure 12 shows the EBS and PD for MgB_2 at 0 GPa and 20 GPa, respectively, and demonstrates a shift in the σ bands at the Fermi level although no loss of degeneracy around **Γ**. The shift of the σ bands to lower energy at 20 GPa is equivalent to ~0.05 eV. In comparison, the PD for MgB_2 under these conditions is more sensitive to pressure as indicated by the relative depth, δ, of the phonon anomaly centred around **Γ**. The change in value for δ is related to the thermal energy, T_δ, of the phonon anomaly [29] and shows a linear relationship with change in pressure up to 20 GPa as well as strong correlation with experimentally determined T_c [11]. In **Figure 12**, the value of δ_1 for MgB_2 at 0 GPa is ~128 cm^{-1} while δ_2 at 20 GPa is ~75 cm^{-1}. These values result in

http://dx.doi.org/10.5772/intechopen.79216

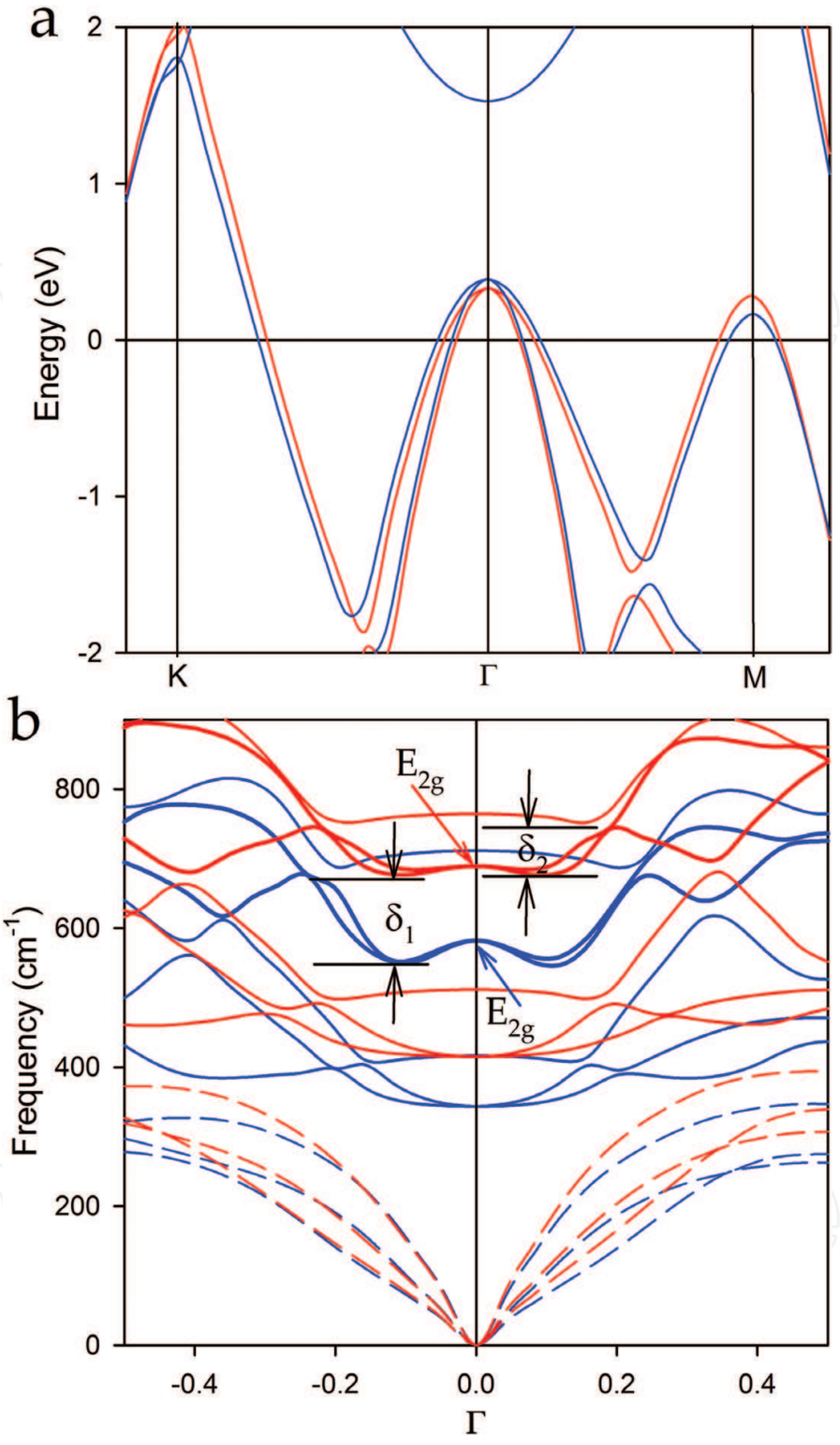


Figure 12. *Ab initio* DFT calculations for MgB_2 at 0 (blue lines) and 20 GPa (red lines) using the LDA functional with $\Delta k = 0.02$ A^{-1} for (a) electronic bands and (b) phonon dispersions centred around **Γ**. Note the substantial change in the depth of the phonon anomaly between 0 (δ_1) and 20 GPa (δ_2) and the higher frequencies for E_{2g} at 20 GPa.

a calculated T_δ ~40 and ~20 K, at 0 and 20 GPa, respectively, consistent with experimentally measured T_c values for MgB_2 [11, 27]. Another expected effect of increased hydrostatic pressure is an overall shift of phonon modes to higher frequency as shown in **Figure 12b**.

The shift of σ bands in the EBS for MgB_2 follows a consistent trend to that observed for other structural variations such as metal substitution and electron density as shown above. Goncharov and Struzhkin [75] suggested on the basis of approximations to the Eliashberg formulation, that degenerate electronic bands split above and below the Fermi level at 20 GPa at which point experimental data diverge slightly from a linear relationship between T_c and P. However, it is clear from these *ab initio* DFT calculations that MgB_2 retains the aforementioned superconductivity characteristics at 20 GPa and experimental data shows superconductivity [27]. With increased pressure, the separation of Fermi surfaces, or the inter-tubular distance as described above, also decreased [11]. While this decrease in inter-tubular distance is subtle, its relationship to the value of δ and appropriate choice of Δk grid resolution provides clarity of interpretation [11, 34] and shows that this region of reciprocal space is key to the determination of superconductivity for MgB_2 and derivative structures [19]. The link between electron and phonon behaviour in MgB_2, including the onset of superconductivity, is well modelled using *ab initio* DFT for a wide range of equivalent experimental conditions.

5.3. Prediction using DFT

The foregoing description of computational outcomes facilitated by a consistent *ab initio* DFT methodology using the same functionals to achieve convergent PDs across a wide range of conditions and compositions implies that the approach is suited to predicting electronic properties of other diborides, and perhaps, other structure types. Furthermore, the obvious but oft forgotten interdependence of the EBS and the PD of solids suggests that the strong electron–phonon interactions of BCS superconductors are calculable without modification and are predictable.

Implicit prediction of T_c for metal substituted MgB_2 occurred soon after the announcement by Nagamatsu et al. [21] and took the form of syntheses with hole doped additions that, in general, led to a decrease in T_c compared with the parent compound [31, 77]. However, other researchers used the Eliashberg formulation to show that Na and/or Ca substitution into MgB_2 would increase T_c [78] but there is little evidence to suggest that Na, for example, is soluble in MgB_2 [79] and, to date, a Na-substituted MgB_2 has not been synthesised. More recently, the depth of the phonon anomaly at **Γ** has been used to calculate the T_δ of "unknown" metal substituted MgB_2 as well as other compounds such as BaB_2 [29, 30]. For BaB_2, the PD does not converge until a hydrostatic pressure ~16 GPa is applied at which the estimated T_δ is between ~60 and ~80 K depending on the linear response method chosen [29]. Using a similar strategy, Ba-substituted MgB_2 shows a T_δ ranging between ~62 and ~64 K (± ~6 K) depending on the level of substitution [29]. To date, clear evidence for synthesis of these specific modelled compositions is not extant.

As noted above, Palnichenko et al. [74] report syntheses of MgB_2 in the presence of Rb, Cs and Ba which, on the basis of ^{11}B NMR data, suggests substitution of these elements into the MgB_2 structure in a proportion of the product. Measurement of T_c using ac susceptibility shows possible onsets of superconductivity at 52, 58 and 45 K, respectively in the products. Despite the difficulty in interpreting the NMR data in terms of specific crystal structure(s), the implication from this experimental work—among the few reported attempts at charge carrier donation—is

http://dx.doi.org/10.5772/intechopen.79216

that Ba substitution into MgB_2 has increased T_c above that for MgB_2 [74]. The trend of this experimental work is consistent with the outcomes calculated for T_δ from the PDs of $Mg_{1-x}Ba_xB_2$ [29, 30] and suggests that *a priori* prediction of T_c for unknown, or "new," compounds is achievable.

6. Superlattices

Consideration of superlattices derived from a primary structural model provides an effective interpretation of fine-scale experimental data that reflect dynamic atom (or electron-ion core) interactions in the solid state. A superlattice may enable facile resolution of computational models that invoke atom substitution or show dynamic symmetry conditions manifest in subtle shifts of electron density within a structure and that are detectable using experimental techniques such as Raman spectroscopy. In principle, the textbook superlattice example is of the mass modulation of a linear chain of identical masses denoted by m [3, 10]. The original mass m, separated by equal distances *a*, displays only acoustic modes of vibration, which have a group velocity related to the sound velocity. When a modulation of the masses is introduced through masses m and M, the new real space periodicity becomes 2*a*, resulting in a folding of reciprocal space at half the reciprocal space Π/2*a*. This action introduces the so called optic modes that have flatter dispersions than the acoustic modes as demonstrated in the PDs above. Similar behaviour can also be attributed to a modulation of the forces between identical masses [80] and this is exemplified by the phonon response to bond deformation in MgB_2 as shown above.

Nevertheless, interpretation of these phenomena, particularly when dissecting the richness of current generation DFT models, requires careful attention to the following:

a. Multiplicity: When a superlattice is constructed, the number of atoms in the cell are multiplied by the integer order of the superlattice. Thus, the number of degrees of freedom 3 N for N atoms is multiplied accordingly. This multiplicity can result in very complex EBSs and PDs that are difficult to interpret in a practical manner and, of course, significantly increases the computational payload required for a calculation.

b. Folding of reciprocal space: Original values or modes at a boundary zone become folded and part of the spectrum of the superlattice **Γ** point. While folding will bring about beneficial information for modest sized superlattices (as shown above for MgB_2), interpretation of models for very large superlattices may also become complex, particularly for low symmetry structures.

c. Computational resolution: PD calculations are particularly sensitive to Δk grid resolution in that a phonon anomaly may not be evident or may have a very irregular appearance if the interval for **k** is too coarse [13, 34].

With attention to the above caveats, DFT is an excellent tool for real space interpretation of solid state phenomena that respond to variations in electron distributions induced by external factors.

7. Conclusions

Ab initio DFT models of electron and phonon behaviour in superconducting materials provide powerful tools for interpretation of existing, known compounds as well as for prediction of new compositions that may demonstrate novel, or desired, conduction properties. The full capacity of DFT, manifest in EBS and PD reciprocal space representations, when considered together for a particular compound provides unambiguous indication of potential for superconductivity as well as a credible estimate of T_c and an estimate of error for T_c. Either an EBS or PD alone may be sufficient to indicate superconductivity—for BCS-type materials—but both representations are necessary for minimal ambiguity. In particular, for AlB_2-type structures degenerate parabolic σ bands focused at a crystallographic boundary above the Fermi level and with split bands at the Fermi level are *a priori* indicators of superconductivity, or that superconductivity is a strong possibility with fine-tuning of the structure. In addition, a phonon anomaly of the optical E_{2g} modes degenerate at **Γ** is similarly an *a priori* indicator of superconductivity in AlB_2-type structures. We have applied these basic principles to other high symmetry compounds (e.g. cubic or tetragonal superconductors and/or insulators) with similar interpretative clarity particularly when transcribed to real space configurations. To experimentally validate these principles across all superconductor families, and to design new predictive targets for synthesis, requires real space descriptions of compounds for rapid evaluation of appropriate synthesis techniques. We encourage further systematic and critical comparisons of the known 32 families of superconductors [81] using these DFT tools.

Acknowledgements

This research did not receive any specific grant from funding agencies in the public, commercial or not-for-profit sectors. Access to, and ongoing assistance with, QUT's HPC facilities particularly from Ashley Wright, Abdul Sharif and Hamish Macintosh, is gratefully acknowledged. The authors are grateful to Associate Professor Alexey Kolmogorov for alerting them to the results in the article by Palnichenko et al. [74].

Author details

Jose A. Alarco and Ian D.R. Mackinnon*

*Address all correspondence to: ian.mackinnon@qut.edu.au

Institute for Future Environments and Science and Engineering Faculty, University of Technology (QUT), Brisbane, Queensland, Australia

References

[1] Urch DS. Orbitals and Symmetry. Harmondsworth, Middlesex, England: Penguin Books Ltd; 1970

[2] Brandt NB, Chudinov SM. Electronic Structure of Metals. Moscow: Mir Publishers; 1975

[3] Ziman JM. Electrons and Phonons: The Theory of Transport Phenomena in Solids. Oxford: Oxford University Press; 1960

[4] Born M, Huang K. Dynamical Theory of Crystal Lattices Oxford Classic Texts in the Physical Sciences. Oxford: Clarendon Press; 1988

[5] Ziman JM. Principles of the Theory of Solids. 2nd ed. Cambridge: Cambridge University Press; 1972

[6] Kohn W. Nobel lecture: Electronic structure of matter—Wave functions and density functionals. Reviews of Modern Physics. 1999;**71**(5):1253-1266

[7] Giustino F. Materials Modelling Using Density Functional Theory—Properties and Predictions. Oxford: Oxford University Press; 2014

[8] Born M, Oppenheimer R. Zur Quantentheorie der Molekeln. Annalen der Physik. 1927;**4**(84):457-484

[9] Altmann SL. Band Theory of Solids: An Introduction from the Point of View of Symmetry. Oxford: Clarendon Press; 2002

[10] Sherwood PMA. Vibrational Spectroscopy of Solids. Cambridge: Cambridge University Press; 1972

[11] Alarco JA, Talbot PC, Mackinnon IDR. Phonon dispersion models for MgB_2 with application of pressure. Physica C: Superconductivity and Its Applications. 2017;**536**:11-17

[12] Singh PP. From E_{2g} to other modes: Effects of pressure on electron-phonon interaction in MgB_2. Physical Review Letters. 2006;**97**(24):247002

[13] Heid R, Bohnen K-P, Renker B. Electron-phonon coupling and superconductivity in MgB_2 and related diborides. Advances in Solid State Physics. 2002;**42**:293-305

[14] Bardeen J, Cooper LN, Schrieffer JR. Theory of superconductivity. Physics Review. 1957;**108**:1175-1204

[15] Duan F, Guojun J. Introduction to Condensed Matter Physics. Vol. 1. Singapore: World Scientific; 2007

[16] Mourachkine A. Room-Temperature Superconductivity. Cambridge: Cambridge International Science Publishing; 2004

[17] Wilson EBJ, Decius JC, Cross PC. Molecular Vibrations—The Theory of Infrared and Raman Vibrational Spectra. New York: Dover Publication, Inc.; 1955

[18] Geballe TH, Hammond RH, Wu PM. What T-c tells. Physica C: Superconductivity and Its Applications. 2015;**514**:9-16

[19] Alarco JA, Talbot PC, Mackinnon IDR. A complete and accurate description of superconductivity of AlB2-type structures from phonon dispersion calculations. Journal of Superconductivity and Novel Magnetism. 2018;**31**:727-731

[20] Carbotte JP. Properties of boson exchange superconductors. Reviews of Modern Physics. 1990;**62**(4):1027-1157

[21] Nagamatsu J, Nakagawa N, Muranaka T, Zenitani Y, Akimitsu J. Superconductivity at 39 K in magnesium diboride. Nature. 2001;**410**:63-64

[22] Jorgensen JD, Hinks DG, Short S. Lattice properties of MgB_2 versus temperature and pressure. Physical Review B. 2001;**63**(224522):1-5

[23] Narlikar A. Superconducting magnesium diboride. In: Studies of High Temperature Superconductors. Vol. 38. New York: NOVA Science Publishers Inc.; 2002. 514pp

[24] Buzea C, Yamashita T. Topical review—Review of the superconducting properties of MgB_2. Superconductor Science and Technology. 2001;**14**:R115-R146

[25] Alarco JA, Talbot PC, Mackinnon IDR. Coherent phonon decay and the boron isotope effect for MgB_2. Physical Chemistry Chemical Physics. 2014;**16**(46):25386-25392

[26] Hinks DG, Claus H, Jorgensen JD. The complex nature of superconductivity in MgB_2 as revealed by the reduced total isotope effect. Nature. 2001;**411**(6836):457-460

[27] Deemyad S et al. Dependence of the superconducting transition temperature of single and polycrystalline MgB_2 on hydrostatic pressure. Physica C: Superconductivity. 2003;**385**(1):105-116

[28] Tang J et al. Lattice parameter and T_c dependence of sintered MgB_2 superconductor on hydrostatic pressure. Physical Review B. 2001;**64**(13):132509

[29] Alarco JA, Talbot PC, Mackinnon IDR. Phonon anomalies predict superconducting T_c for AlB_2-type structures. Physical Chemistry Chemical Physics. 2015;**17**(38):25090-25099

[30] Mackinnon IDR, Talbot PC, Alarco JA. Phonon dispersion anomalies and superconductivity in metal substituted MgB_2. Computational Materials Science. 2017;**130**:191-203

[31] Karpinski J, Zhigadlo ND, Katrych S, Puzniak R, Rogacki K, Gonnelli R. Single crystals of MgB_2: Synthesis, substitutions and properties. Physica C. 2007;**456**:3-13

[32] Agrestini S et al. Sc doping of MgB_2: The structural and electronic properties of $Mg_{1-x}Sc_xB_2$. Journal of Physics and Chemistry of Solids. 2004;**65**(8-9):1479-1484

[33] Agrestini S et al. Substitution of Sc for Mg in MgB_2: Effects on transition temperature and Kohn anomaly. Physical Review B. 2004;**70**(13):134514

[34] Alarco JA, Chou A, Talbot PC, Mackinnon IDR. Phonon modes of MgB_2: Super-lattice structures and spectral response. Physical Chemistry Chemical Physics. 2014;**16**:24443-24456

[35] Alarco JA, Talbot PC, Mackinnon IDR. Electron density response to phonon dynamics in MgB_2: An indicator of superconducting properties. Modelling and Numerical Simulation of Material Science. 2018;**8**:21-46

[36] Martin RM. Electronic Structure—Basic Theory and Practical Methods. Cambridge: Cambridge University Press; 2005

[37] Xi XX. Two-band superconductor magnesium diboride. Reports on Progress in Physics. 2008;**71**(116501):26

[38] Almutairi A, Zhang C, Du A, Lipton-Duffin J, Farrell T, Alarco JA. Approximate parabolic and tight binding equations for the electronic bands of MgB_2 under a range of external conditions. submitted 2018, under review. 2018;**31**:727-731

[39] Phillips JC. Bonds and Bands in Semiconductors. New York, London: Academic Press; 1973

[40] Sutton AP. Electronic Structure of Materials. Oxford: Clarendon Press - Oxford Science Publications; 2004

[41] Kohn W. Image of the Fermi surface in the vibration spectrum of a metal. Physical Review Letters. 1959;**2**(9):393-394

[42] Baron AQR et al. Kohn anomaly in MgB_2 by inelastic X-ray scattering. Physical Review Letters. 2004;**92**(19):19700

[43] Baron AQR et al. Review: Phonon spectra in pure and carbon doped MgB_2 by inelastic X-ray scattering. Physica C. 2007;**456**:83-91

[44] Accelrys. Materials Studio CASTEP Online Help: "Requesting Vibrational Properties". Available from: http://www.tcm.phy.cam.ac.uk/castep/documentation/WebHelp/html/tskcastepreqvibprops.htm

[45] Xiang JY et al. Superconducting properties and c-axis superstructure of $Mg_{1-x}Al_xB_2$. Physical Review B. 2002;**65**:214536

[46] Zandbergen HW, Wu MY, Jiang H, Hayward MA, Haas MK, Cava RJ. The complex superstructure in $Mg_{1-x}Al_xB_2$ at x~0.5. Physica C. 2002;**366**:221-228

[47] Li JQ, Li L, Liu FM, Dong C, Xiang JY, Zhao ZX. Superconductivity, superstructure, and structure anomalies in $Mg_{1-x}Al_xB2$. Physical Review B. 2002;**65**:132505

[48] Blaha P, Schwarz K, Luitz J. WIEN2k-FAQ: Positive Fermi Energy: What Does it Mean? 2001. Available from: http://susi.theochem.tuwien.ac.at/reg_user/faq/neg_fermi_energy.html

[49] Escamilla R et al. Crystalline structure and the superconducting properties of NbB_{2+x}. Journal of Physics: Condensed Matter. 2004;**16**:5979-5990

[50] Machado AJS, Renosto ST, dos Santos CAM, Alves LMS, Fisk Z. Defect structure versus superconductivity in MeB_2 compounds (Me = refractory metals) and one-dimensional superconductors. In: Gabovich A, editor. Superconductors—Materials, Properties and Applications. London: InTechOpen; 2012. pp. 45-60

[51] Renosto ST et al. Evidence of multiband behavior in the superconducting alloy $Zr_{0.96}V_{0.04}B_2$. Physical Review B. 2013;**87**(174502):1-6

[52] Jung S-G et al. Critical current density and flux pinning in $Zr_{0.96}V_{0.04}B_2$ superconductor with AlB_2 structure. Journal of Applied Physics. 2013;**114**(133905):1-4

[53] Marques MDR et al. Study of the superconducting properties of the new intermetallic compound $Zr_{1-x}Nb_xB_2$. Superconductor Science and Technology. 2016;**95007**:1-6

[54] Pickett WE, An JM, Rosner H, Savrasov SY. Role of two dimensionality in MgB_2. Physica C. 2003;**387**:117-121

[55] An JM, Pickett WE. Superconductivity of MgB_2: Covalent bonds driven metallic. Physical Review Letters. 2001;**86**(19):4366-4369

[56] Sichkar SM, Antonov VM. Electronic structure, phonon spectra and electron–phonon interaction in ScB_2. Low Temperature Physics. 2013;**39**(7):595-601

[57] Chen K et al. Properties of MgB_2 films grown at various temperatures by hybrid physical–chemical vapour deposition. Superconductor Science and Technology. 2008;**21**(9):095015

[58] Kim Y-S, Shin H-S. Preparation and characterization of magnesium diboride superconductor by melting process. Korean Journal of Chemical Engineering. 2003;**20**(6):1183-1187

[59] Grasso G et al. Transport properties of powder-in-tube processed MgB_2 tapes. Physica C. 2002;**378-381**:899-902

[60] Malagoli A, Braccini V, Scati N, Roncallo S, Siri AS, Grasso G. Fabrication and superconducting properties of powder-in-tube processed MgB_2 tapes. Physica C. 2002;**372-376**: 1245-1247

[61] Cava RJ, Zandbergen HW, Inumaru K. The substitutional chemistry of MgB_2. Physica C. 2003;**385**:8-15

[62] Bud'ko SL, Canfield PC. Superconductivity of magnesium diboride. Physica C: Superconductivity and Its Applications. 2015;**514**:142-151

[63] Mackinnon IDR, Winnett A, Alarco JA, Talbot PC. Synthesis of MgB_2 at low temperature and autogenous pressure. Materials. 2014;**7**(5):3901-3918

[64] Hlinka J et al. Phonons in MgB_2 by polarized Raman scattering on single crystals. Physical Review B. 2001;**64**:140503

[65] Quilty JW, Lee S, Yamamoto A, Tajima S, Yamanaka A. A Raman scattering study of superconductivity in MgB_2. Physica C. 2003;**388-389**:131-132

[66] Campi G et al. Study of temperature dependent atomic correlations in MgB_2. European Physical Journal B. 2006;**52**(1):15-21

[67] Pena O. Chevrel phases: Past, present and future. Physica C: Superconductivity and Its Applications. 2015;**514**:95-112

[68] Fournier P. T′ and infinite-layer electron-doped cuprates. Physica C: Superconductivity and Its Applications, Review. 2015;**514**:314-338

[69] Chu CW, Deng LZ, Lv B. Hole-doped cuprate high temperature superconductors. Physica C: Superconductivity and Its Applications. 2015;**514**:290-313

[70] Schilling JS. What high pressure studies have taught us about high-temperature superconductivity. In: Frontiers of High Pressure Research II: Application of High Pressure to Low-Dimensional Novel Electronic Materials. Springer Netherlands, Dordrecht: Springer; 2001. pp. 345-360

[71] Hinks DG, Jorgensen JD, Zheng H, Short S. Synthesis and stoichiometry of MgB_2. Physica C. 2002;**382**:166-176

[72] Karpinski J et al. Al substitution in MgB_2 crystals: Influence on superconducting and structural properties. Physical Review B. 2005;**71**(17):174506

[73] Lee BW, Choia I, Junga CU, Leeb SI. Doping in MgB_2 superconductors using a high-pressure furnace. Journal of Magnetism and Magnetic Materials. 2008;**320**:e484-e486

[74] Palnichenko AV, Vyaselev OM, Sidorov NS. Influence of Rb, Cs, and Ba on the superconductivity of magnesium diboride. JETP Letters. 2007;**86**(4):272-274

[75] Goncharov AF, Struzhkin VV. Pressure dependence of the Raman spectrum, lattice parameters and superconducting critical temperature of MgB_2: Evidence for pressure-driven phonon-assisted electronic topological transition. Physica C: Superconductivity. 2003;**385**(1-2):117-130

[76] Goncharov AF et al. Raman spectrum and lattice parameters of MgB_2 as a function of pressure. Physical Review B. 2001;**64**(10):100509

[77] Karpinski J et al. MgB_2 single crystals substituted with Li and with Li-C: Structural and superconducting properties. Physical Review B. 2008;**77**(21):214507

[78] Neaton JB, Perali A. On the Possibility of Superconductivity at Higher Temperatures in sp-Valent Diborides. arXiv:Cond-Mat/0104098 [Cond-Mat.Supr-Con]; 2001. pp. 1-27

[79] Mackinnon IDR, Shahbazi M, Alarco JA, Talbot PC. Low temperature decomposition of metal borohydride drives autogenous synthesis of MgB_2. Superconductor Science and Technology. 2017;**30**:055004

[80] Janot C. Quasicrystals—A Primer. Oxford: Clarendon Press - Oxford Science Publications; 1997

[81] Hirsch JE, Maple MB, Marsiglio F. Superconducting materials classes: Introduction and overview. Physica C: Superconductivity and Its Applications. 2015;**514**:1-8

IntechOpen

IntechOpen